

## Supplementary Information

### Soluble polyimide-based colorless-to-orange–red switching electrochromic film by incorporating universal joint-like structure

*Xiaoqing Sun<sup>a,b,c</sup>, Chongwen Yu<sup>b,c</sup>, Xingyao Liu<sup>a,b,c</sup>, Taolve Wang<sup>b,c</sup>, Xigao Jian<sup>a</sup>, Yujie Song<sup>b,c\*</sup>,  
Jian Xu<sup>a,b,c\*</sup>*

<sup>a</sup> State Key Laboratory of Fine Chemicals, Liaoning High Performance Polymer Engineering Research Center, School of Chemical Engineering, Dalian University of Technology, Dalian 116024, China

<sup>b</sup> Zhejiang Key Laboratory of Data-Driven High-Safety Energy Materials and Applications, Ningbo Key Laboratory of Special Energy Materials and Chemistry, Ningbo Institute of Materials Technology and Engineering, Chinese Academy of Sciences, Ningbo 315201, China

<sup>c</sup> Qianwan Institute of CNITECH, Ningbo 315336, China

\* Corresponding authors: xujian1028@dlut.edu.cn (J. Xu)

## 1 Instruments and characterization

The  $^1\text{H}$  NMR and  $^{13}\text{C}$  NMR spectra were recorded on a Bruker AVANCE NEO spectrometer, using tetramethylsilane (TMS) as an internal standard. Samples were tested in either 0.5 mL deuterated dimethyl sulfoxide ( $\text{DMSO-}d_6$ ) at a temperature of 25 °C.

The Fourier transform infrared (FT-IR) spectra were collected on a Bruker INVENIOR FT-IR spectrometer, using a potassium bromide (KBr) baseline, within the spectral range of 4000-500  $\text{cm}^{-1}$ , with 64 scans.

The Matrix-assisted laser desorption ionization time-of-flight tandem mass spectrometry (MALDI-TOF-MS) was performed on a Bruker Ultraflex extreme instrument with a 355 nm Nd:YAG laser, using an MTP384 stainless steel unpolished target plate.

The X-ray diffraction (XRD) analysis was conducted on a Bruker ADVANCE D8, scanning from 5° to 80° at a rate of 2°  $\text{min}^{-1}$ , with a Cu K $\alpha$  radiation source.

The thermogravimetric analysis (TGA) was performed on a Netzsch STA449F3 instrument under argon or air atmosphere with a flow rate of 20  $\text{mL min}^{-1}$ , in the temperature range of 50 °C to 1000 °C, at a heating rate of 10 °C  $\text{min}^{-1}$ .

The differential scanning calorimetry (DSC) was conducted on a TA Q250 instrument under a nitrogen atmosphere with a flow rate of 20  $\text{mL min}^{-1}$ , in the temperature range of 50 °C to 400 °C, at a heating rate of 10 °C  $\text{min}^{-1}$ .

The scanning electron microscopy (SEM) was performed on an FEI Hitachi SU8220 to characterize the thickness of the polymer working electrode. During testing, the glass portion of the film/ITO electrode was attached to the SEM sample stage using conductive adhesive, and the sample was sputter-coated with gold before observation. Atomic force microscopy (AFM) was conducted on Bruker Dimension Icon to characterize the surface roughness of the THZ-PI film.

Ultraviolet-visible (UV-vis) spectrophotometer was conducted on a PerkinElmer Lambda 1050+ spectrometer. The optical properties of THZ-PI in different solutions and solid films were carried out in diluted polymer solutions ( $10^{-5}$  M of *N,N*-dimethylformamide, dichloromethane or tetrahydrofuran in polymer solution) as well as films obtained by spin-coating the dichloromethane solution on conductive glass by drop-coating technique.

The solubility of polyimide was qualitatively evaluated by the solubility of 10 mg of THZ-PI powder in 1 mL of solvent, and observing the state of the solution after placing it at room temperature for 24 h.

The electrochemical properties were evaluated through cyclic voltammetry (CV) and electrochemical impedance spectroscopy (EIS) using a CHI660E electrochemical workstation from CH Instruments, Shanghai, China, using a three-electrode system. The PTZ-PI/ITO served as the working electrode, a platinum plate as the counter electrode, and Ag/AgCl as the reference electrode, with a 0.1 M tetrabutylammonium perchlorate (TBAP) in acetonitrile (CH<sub>3</sub>CN) as the electrolyte. For electrochromic testing, the UV-vis spectrometer was coupled with the electrochemical workstation. The polyimide/ITO electrode was placed in a cuvette, using the same reference electrode, counter electrode, and electrolyte as in the electrochemical test. A gradually increasing or square-wave voltage was applied to the polymer film, while changes in parameters such as absorbance or transmittance of the polymer film were monitored using the UV-vis spectrophotometer. The electrochromic cycling stability test was conducted using the Chronoamperometry (CA) mode of the electrochemical workstation, where a square-wave voltage was applied within the potential range determined in potential-dependent UV-vis absorption spectra. The test was performed with a cycle duration of 15 s, and the cycling stability at three wavelengths was evaluated for each material over a period of 3600 s.

Through theoretical analysis, the relationship between their structure and properties could be further revealed. The Gaussian 16 was used for all calculations, and Gauss View 6.0 was used for visual analysis. Based on the optimized ground state, the three-dimensional structure of the monomer unit, HOMO and LUMO orbital distribution of the monomer were calculated by using the B3LYP exchange-correlation functional and the 6-31++G (d, p) basis set, and the electrostatic potential (ESP) diagram was visualized. Then, based on the same theoretical level, the excitation energy and oscillator intensity of 20 singlet transitions were calculated by Time-Dependent Density Functional Theory (TD-DFT), and the UV-vis spectrum were simulated.

## 2 Monomer synthesis

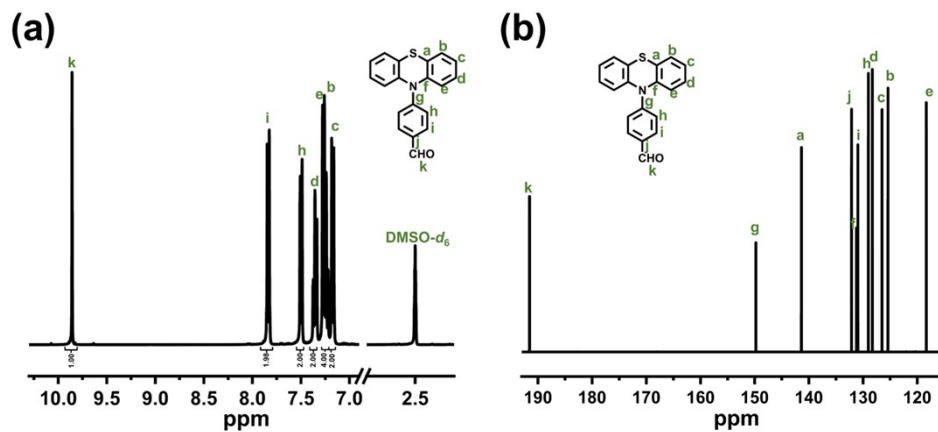


Fig. S1 (a)  $^1\text{H}$  NMR spectrum; (b)  $^{13}\text{C}$  NMR spectrum of THZ-AL.

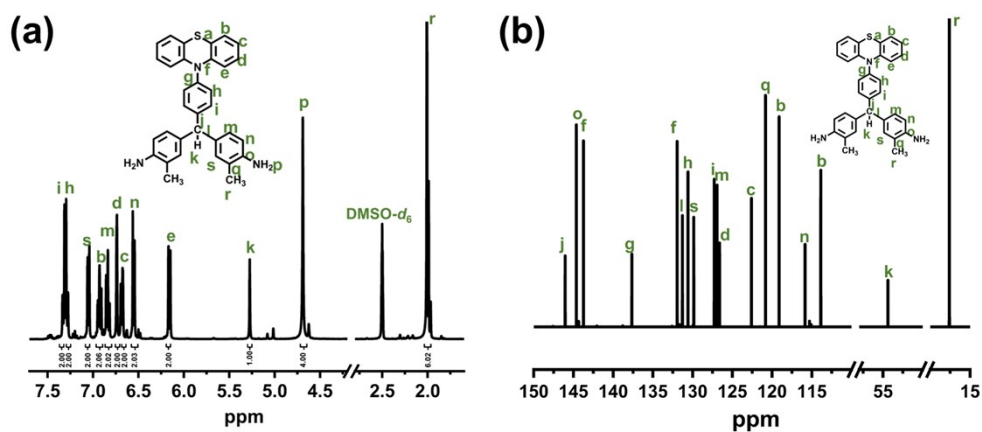


Fig. S2 (a)  $^1\text{H}$  NMR spectrum; (b)  $^{13}\text{C}$  NMR spectrum of THZ-DA.

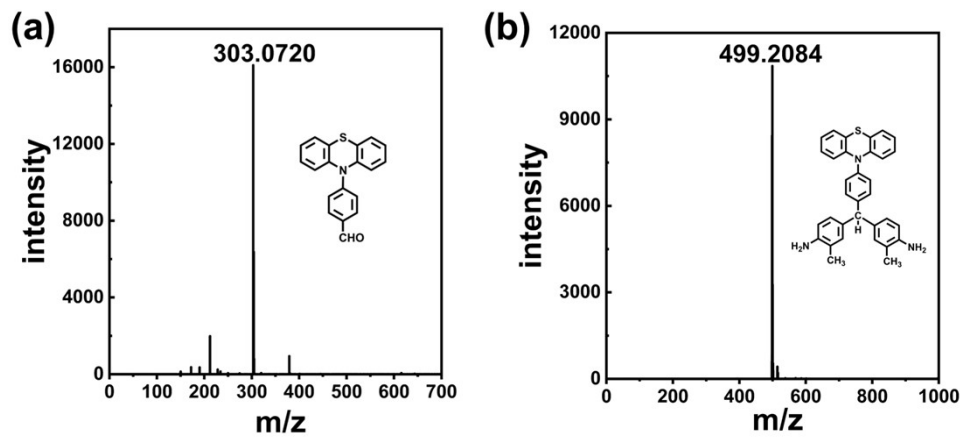


Fig. S3 MALDI-TOF-MS spectra of (a) THZ-AL; (b) THZ-DA.

### 3 The polymer polymerization

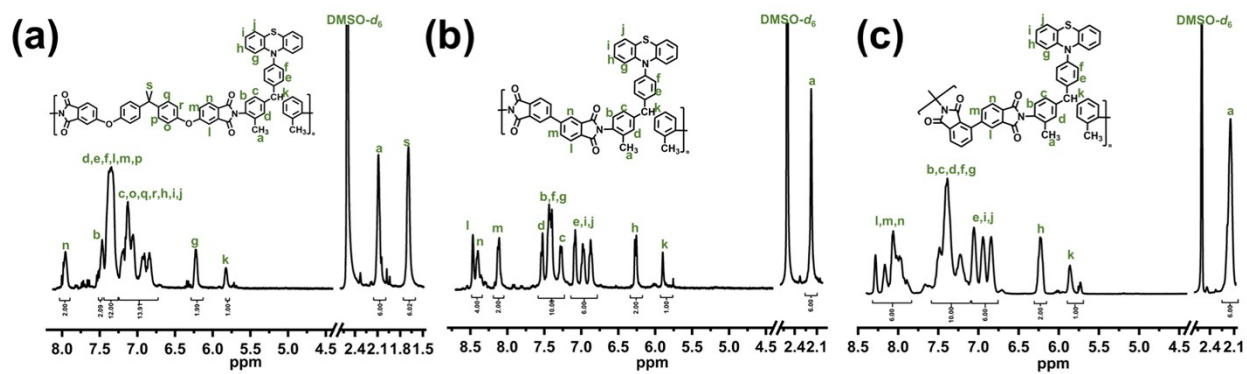


Fig. S4  $^1\text{H}$  NMR spectra of (a) THZ-a; (b) THZ-b; (c) THZ-c.

## 4 Thermal properties of THZ-PIs

**Table S1** Thermal properties of THZ-PIs

THZ-PI code	$T_g$ (°C)	$T_{d5\%}$ (°C)		Char yield (%)	
		in Ar	in air	in Ar	in air
THZ-a	248	424	461	59	1
THZ-b	347	407	430	65	3
THZ-c	319	370	437	63	0.7

## 5 Optical properties of THZ-PIs

**Table S2** Optical properties of THZ-PIs

THZ-PI code	$\lambda_{\text{cut-off}}$ <sup>a</sup>	$T_{305}$ (%) <sup>b</sup>	$T_{420}$ (%) <sup>c</sup>
THZ-a	309	2.55	79.65
THZ-b	311	1.99	79.56
THZ-c	308	2.39	80.49

<sup>a</sup> The cut-off wavelength in transmittance curve;

<sup>b</sup> The transmittance of THZ-PIs at 305 nm in the transmittance curve;

<sup>c</sup> The transmittance of THZ-PIs at 420 nm in the transmittance curve.

**Table S3** Characteristic wavelengths of UV-vis absorption spectra of THZ-PIs

THZ-PI code	The wavelength corresponding to the absorption peak		
	DMF (nm)	DCM (nm)	THF (nm)
THZ-a	273, 322	323	324
THZ-b	272, 323	318	319
THZ-c	267, 312	313	310

## 6 Solubility behavior of THZ-PIs

**Table S4** Solubility of THZ-PIs

THZ-PI code	Solvent							
	NMP	DMAc	DMF	DCM	CHCl <sub>3</sub>	DMSO	ACE	THF
THZ-a	++	++	++	++	++	+	+	+
THZ-b	++	++	++	++	+	+	+	+
THZ-c	++	++	++	++	++	++	+	++

<sup>a</sup> Solubility : ++, soluble at room temperature; +, soluble on heating; +-, partially soluble or swelling; -, insoluble even on heating;

<sup>b</sup> *N*-methyl-2-pyrrolidone abbreviated for NMP; *N,N*-dimethylacetamide abbreviated for DMAc; *N,N*-dimethylformamide abbreviated for DMF; dichloromethane abbreviated for DCM; chloroform abbreviated for CHCl<sub>3</sub>; dimethyl sulfoxide abbreviated for DMSO; acetone abbreviated for ACE; tetrahydrofuran abbreviated for THF.

## 7 Electrochromic-state-dependent CIE chromaticity coordinate comparison in THZ-PIs

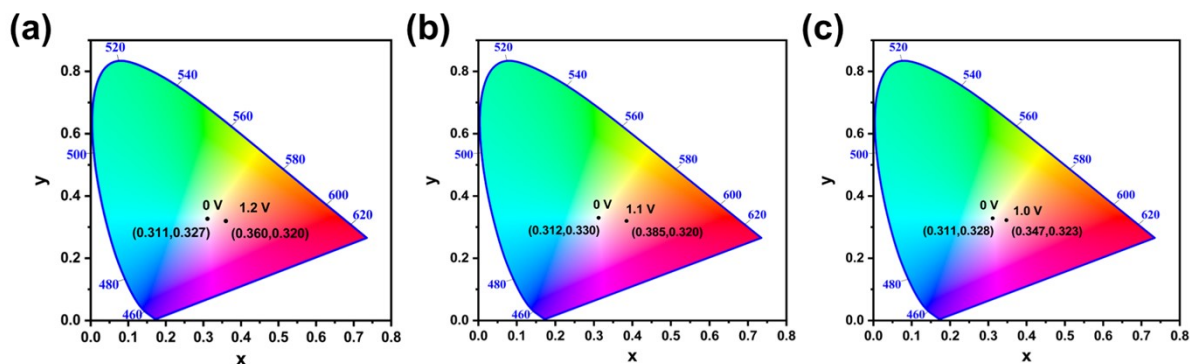


**Fig. S5** Electrochromic-state-dependent CIE chromaticity coordinates (xy) for (a) THZ-a, (b) THZ-b, and (c) THZ-c.

## 8 Electrochromic stability performance of THZ-PIs: retention of optical contrast and current density

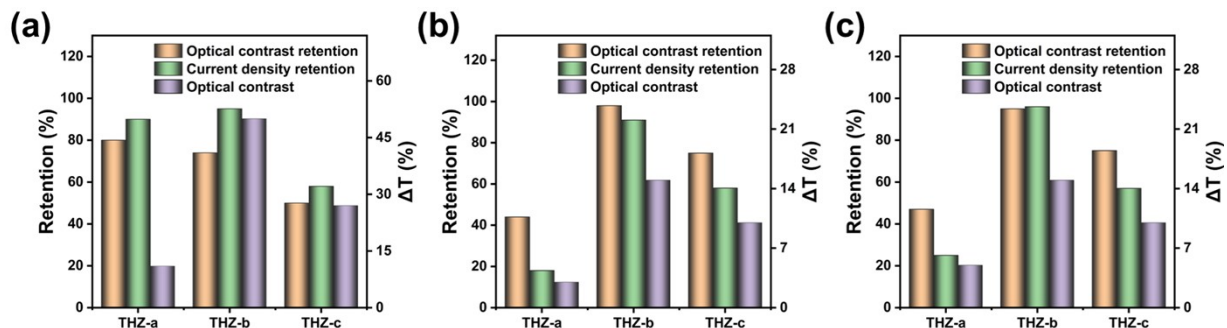


**Fig. S6** The optical contrast ( $\Delta T\%$ ) and electrochromic stability retention (optical contrast and current density) at (a) 519 nm, (b) 782 nm, and (c) 874 nm for THZ-PIs.

**Table S5** The optical contrast ( $\Delta T\%$ ) and electrochromic stability retention (optical contrast and current density) at 519, 782 and 874 nm for THZ-PIs

THZ-PI code	519 nm			782 nm			874 nm		
	Optical contrast		Current density	Optical contrast		Current density	Optical contrast		Current density
	$\Delta T$	retention		$\Delta T$	retention		$\Delta T$	retention	
THZ-a	11%	80%	90%	3%	44%	18%	5%	47%	25%
THZ-b	50%	74%	95%	15%	98%	91%	15%	95%	96%
THZ-c	27%	50%	58%	10%	75%	58%	10%	75%	57%